IOP Conf. Series: Materials Science and Engineering **280** (2017) 012031 doi:10.1088/1757-899X/280/1/012031

Effect of Mechanical Heterogeneity on the Crack Driving Force of a Reactor Pressure Vessel Outlet Nozzle DMW Joint

Zhao Lingyan[1], Cui Yinghao[2] and Xue He[2]

[1]School of Science, Xi'an University of Science and Technology, Xi'an 710054, China
[2]School of Mechanical Engineering, Xi'an University of Science and Technology, Xi'an 710054, China

gloomy2@foxmail.com

Abstract. The welding mechanical heterogeneity, load complexity, material and geometrical structure makes it very difficult to assess the structural integrity of dissimilar metal weld (DMW) joints. Based on a numerical simulated approach of the continuous change of material mechanical property in the buttering layer, a reactor pressure vessel (RPV) outlet nozzle DMW joint with service loads is studied, effect of mechanical heterogeneity on the stress-strain field and stress triaxiality at the semi-elliptical surface crack front are discussed. The analyses show that once the crack extends into the high hardness zone of Alloy 182 buttering, the strain decreases sharply, the strain gradient increases and the crack propagation slows down. The influence of strength mismatch on the stress triaxiality at the shallow crack front is greater than that at the deep crack front. The interaction between strength mismatch and crack depth directly affects the crack growth direction.

1. Introduction

DMW joints are widely used in primary water systems of pressurized water reactors (PWR) [1]. Generally, nickel-based alloy is pre-deposited on the ferritic RPV nozzle face. Then welding is carried out to form a DMW joint with nickel-based alloy. Stress corrosion cracking (SCC) of DMW joints has been paid more attention in the nuclear power industry [2-4]. As a weld filler metal, the high-temperature yield strength of Alloy 182 makes it more susceptible to SCC [5].

The complexity of load, material and geometrical structure also sets obstacles for the structural integrity assessment of DMW joints. And the welding mechanical heterogeneity makes it very difficult to determine the macroscopic fracture parameters at the crack tip [6]. How to simplify the geometry and material properties of DMW joints to increase the assessment reliability is still being studied.

A full-scale 3D finite element model of a RPV outlet nozzle DMW joint under service load, is established based on a continuously changing material model of the buttering layer. Fully considering the mechanical heterogeneity, the stress-strain field and stress triaxiality at the crack front with different crack depth are discussed in detail. The influence of mechanical heterogeneity on the SCC behavior of DMW joints is analyzed, which is of certain engineering value.

2. Finite element modeling

2.1. Specimen model

A typical nozzle safe-end DMW joint to connect the low alloy steel (LAS) nozzles to austenitic stainless steel (SS) pipes is shown in Fig.1, which consists of A508, Alloy 182 buttering, Alloy 182 weld and 304SS. For an axial semi-elliptic crack, c is one half of the crack length and a is the crack depth , the crack angle θ varies from 0º to 180º. The crack parameter c/a is set to be 1.5, and the crack depth a is taken as 5,7.5 and 10 mm, respectively. Preliminary computation results by the elastic-plastic finite element method (EPFEM) show that the Alloy 182 weld and buttering are the high stress zone of the whole component exposed to all the service loads, so it is assumed that a axial semi-elliptical surface crack is located in the Alloy 182 weld.

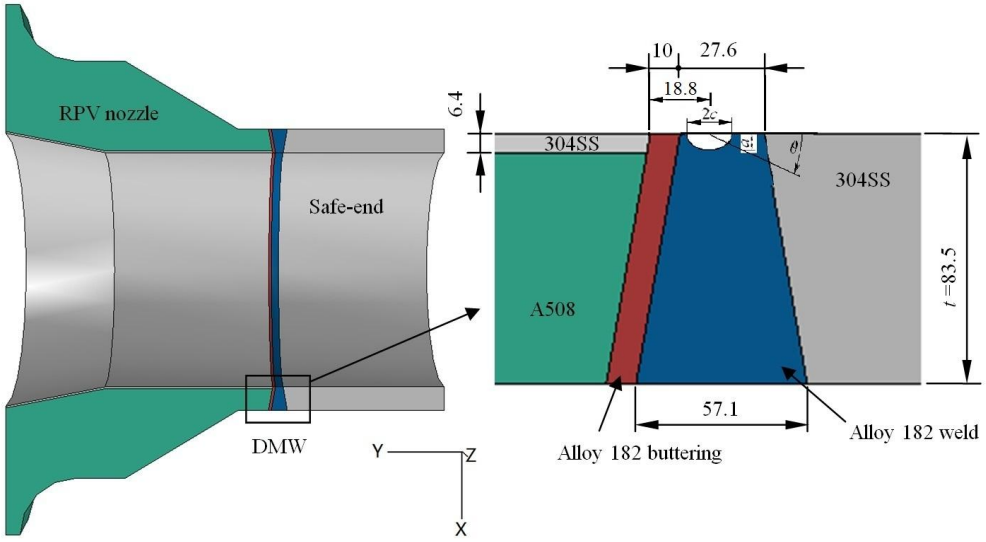

Figure 1. Geometry and material configuration of a DMW joint

2.2. Material model

A typical DMW joint consists of four materials. Their non linear relationship between stress and strain beyond yield is described by Ramberg-Osgood equation in this simulation [7]:

$$\frac{\varepsilon}{\varepsilon_0}=\frac{\sigma}{\sigma_0}+\alpha\left(\frac{\sigma}{\sigma_0}\right)^n \tag{1}$$

Where ε is the strain, including elastic and plastic strain. σ is the total stress; ε_0 is the yield strain of the material, σ_0 is the yield stress of the material, and n is the strain hardening exponent of the material, α is the offset coefficient of the material.

The mechanical properties of the four materials are given in Tab. 1.

Table 1. Material mechanical performance parameters of a DMW joint at 343℃

Material	E /MPa	ν	σ_0 /MPa	n	α
A508	193 000	0.288	440	5.333	1.0
Alloy 182 buttering	193 000	0.288	385~550	4.779~6.617	1.0
Alloy 182 weld	193 000	0.288	385	4.779	1.0
304SS	193 000	0.288	254	4.402	1.0

Following the determination of yield strength, the strain-hardening exponent(n) are estimated according to Eq. (2) [8]:

$$n=\frac{1}{\kappa\ln(1390/\sigma_0)} \tag{2}$$

Where κ=0.163. By using the predefined field module of ABAQUS [9], the material properties of Alloy 182 buttering, for example, yield stress and strain-hardening exponent, become continuously changing parameters [10, 11].

Besides the component gravity force, normal service loads of the DMW joint for RPV nozzles are listed in Tab. 2 [11].

Table 2. Service loads of the DMW joint

Service temperature /℃	Internal pressure /MPa	Axial stress /MPa	Bending moment /kN·m
343	15.59	44	2492

2.3. FE Model

To reduce the computation time, half of the actual structure is selected to establish the 3D finite element model. A symmetry constraint is set on the symmetry plane of the pipe. To reduce the influence of the edge effect on the analysis results, the left and right side of the model are properly extended and fixed constraints are set at the left end according to the Saint-Venant's principle.

Fig.2 gives the mesh of a DMW joint specimen (global model and sub-mode), where X-Y datum is the crack surface and Z-axis is the crack growth direction. 80543 and 41260 8-node linear brick elements are adopted in the global model and sub-model, respectively. A more refined mesh is adopted near the crack front, in order to obtain a more detailed and accurate data. There are 32020 elements in the vicinity of 2 mm around the crack front in the sub-model, more than the half the element total number. The minimum size of the element is about 0.02 mm in the sub-model.

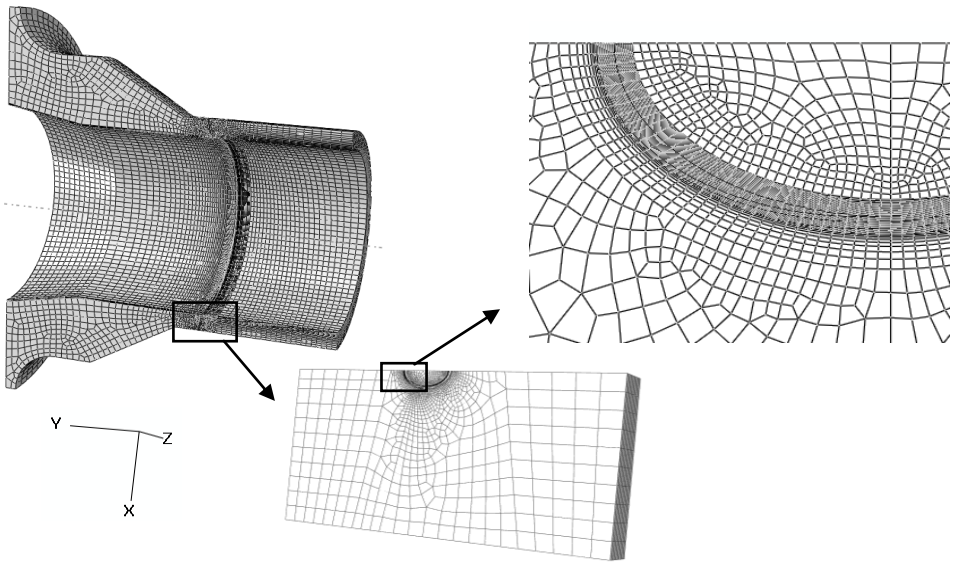

Figure 2. Mesh of the DMW joint

3. Results and Discussion

3.1. Stress and strain around crack front

The tensile stress distribution at the crack front is shown in Fig.3. The stress varies a lot with different crack depths. Due to the yield stress of stainless steel is the smallest among the four material, the high stress zone is close to the stainless steel pipe. Stress of the shallow crack front is the smallest, while high stress area of the deep crack increases greatly, which indicates that the crack has experienced rapid expansion and high stress area is gradually away from the stainless steel pipe.

The tensile plastic strain distribution at the crack front is shown in Fig.4. Similar to the distribution of the open stress, due to low plasticity constraint of the low strength material the high strain zone is close to the stainless steel pipe.

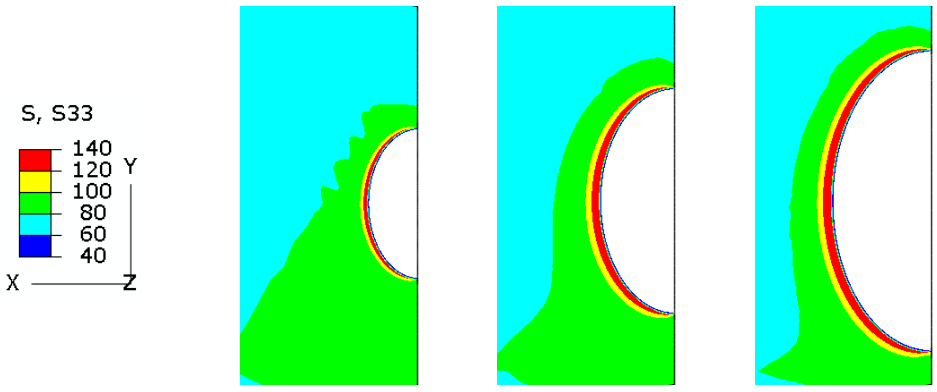

(a) a=5 mm (b) a=7.5 mm (c) a=10 mm

Figure 3. Tensile stress around crack front (MPa)

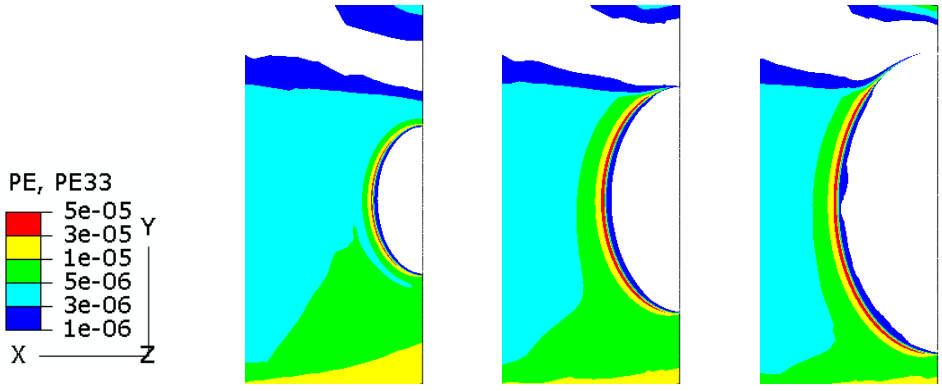

(a) a=5 mm (b) a=7.5 mm (c) a=10 mm

Figure 4. Tensile plastic strain around crack front

Strain at shallow crack front is the smallest and the low strain region appears on the side of the 182 alloy isolation layer. High strain region of the shallow crack front increases much, indicating that the crack has experienced rapid expansion and the high strain zone is close to the stainless steel pipe. Because of stainless steel yield strength is the smallest of all the materials, the largest strain also appears near the side of the stainless steel pipe when the crack depth is10 mm.

3.2. Stress and strain at a certain distance ahead of crack front

Strain and strain rate quickly decrease with the increasing distance ahead of crack tip. A critical issue is to estimate the characteristic distance (r) ahead of crack tip when SCC growth rate is predicted by FRI model [12]. Considering the the stress-strain singularity and comparing the crack tip plastic zones where the equivalent plastic strain is 0.2% with different crack depths, the reasonable distance from crack front is designated as 60 μm in this paper.

The tensile stress at the characteristic distance (r=60 μm) ahead of crack front is shown in Fig.5. Crack propagates gradually and enters the high hardness region of the Alloy 182 buttering with the increase of crack depth. Squeezed by the high strength material. the original flat strain curve appear a peak value, and the stress value is much greater when the crack is deeper. However, the tensile stress ahead of crack front only increases a bit in the Alloy 182 buttering.

The tensile plastic strain at the characteristic distance (r=60 μm) ahead of crack front is shown in Fig.6. The minimum strain occurs when the crack depth is 10 mm. The strain curve ahead of the

shallow crack front extending in the weld metal is flat. The stress increased when the semi-elliptical surface crack is deeper, but the strain reduced drastically and the strain gradient is large, which indicates that the crack propogation in Alloy 182 buttering will slow down.

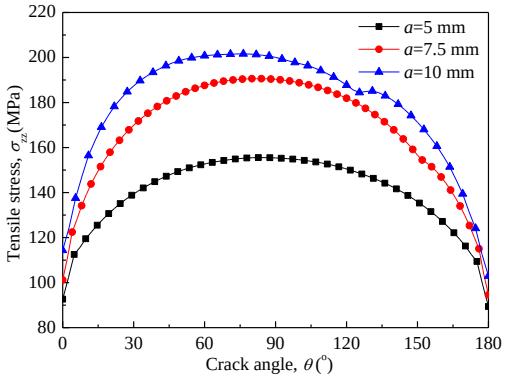

Figure 5. Tensile stress ahead of crack front (MPa)

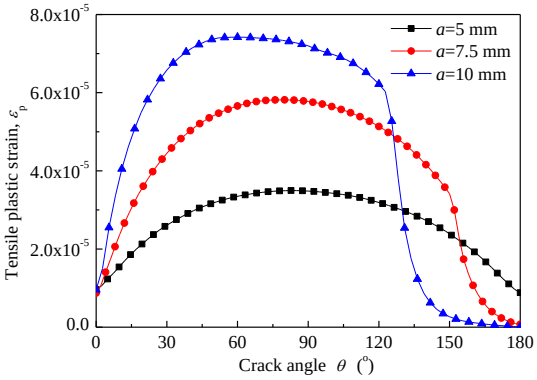

Figure 6. Tensile plastic strain ahead of crack front

3.3. Stress triaxiality ahead of crack front

Research shows that the distribution of the stress triaxiality in the crack front zone may have a great influence on the fracture behavior [13]. The stress triaxiality is described by σ_h/σ_e,, where σ_h denotes the hydrostastic stress and σ_e denotes the equivalent Von-Mises stress.

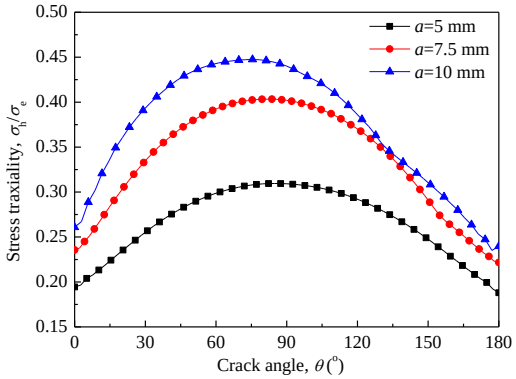

Figure 7. Stress triaxiality ahead of crack front

Stress triaxiality at the characteristic distance (r=60 μm) ahead of crack front is shown in Fig.7. At the same stress loading level, The maximum stress triaxiality occurs when the crack depth is 10 mm.. The high stress triaxiality at the interface region leads to a decrease of the local region toughness. A high stress triaxiality occurs in the low-strength material region due to its low plastic constraint. The high plastic strain zone is consistent with the high stress triaxiality. The local high plasticity strain is coincidence with local high stress triaxiality, which leads to the change of crack propagation direction.

4. Conclusion

Numerical simulation technology is commonly used to analyze piping welded joints that contain irregular crack under service loads. Based on a numerical simulated approach of the continuous change of material mechanical property in Alloy 182 buttering, the stress-strain field and stress triaxiality along the inner surface axial crack front of a RPV outlet nozzle DMW joint are simulated by using EPFEM, conclusions are as follows:

(1) The stainless steel pipe side is the potential direction of crack growth. Once the crack extends into the high hardness zone of Alloy 182 buttering, the strain decreases sharply, the strain gradient increases and the crack propagation slows down.

(2) Due to its low plastic constraint, high stress triaxiality, which occurs in the low-strength material region, leads to a decrease of the local region toughness at the interface region.

(3) The influence of strength mismatch on the stress triaxiality at the shallow crack front is greater than that at the deep crack front. The interaction between strength mismatch and crack depth directly affects the crack growth direction.

Acknowledgments
This work is financially supported by the National Natural Science Foundation of China (Grant nos. are 11502195 and 51475362).

References

[1] Bamford W and Hall J. A review of Alloy 600 cracking in operating nuclear plants including Alloy 82 and 182 weld behavior[C]. *ASME 12th International Conference on Nuclear Engineering*, 2004: 131-139.

[2] Li G F and Congleton J. Stress corrosion cracking of a low alloy steel to stainless steel transition weld in PWR primary waters at 292℃[J]. *Corros. Sci.*, 2000, 42(6): 1005-1021.

[3] Li G F, Li G J, Fang K and Peng J. Stress corrosion cracking behavior of dissimilar metal weld A508/52M/316L in high temperature water environment[J]. *Acta. Metall. Sin*., 2011, 47(7): 797-803.

[4] Bamford W, Newton B and Seeger D. Recent experience with weld overlay repair of indications in Alloy 182 butt welds in two operating PWRS[C]. *ASME 2006 Pressure Vessels and Piping/ICPVT-11 Conference*. 2006: 427-434.

[5] Andresen P, Young L, Horn R and Emigh P. Stress corrosion crack growth rate behavior of Ni Alloys 182 and 600 in high temperature water[J]. *Corros*., 2002.

[6] He X, Ogawa K and Shoji T. Effect of welded mechanical heterogeneity on local stress and strain ahead of stationary and growing crack tips[J]. *Nucl. Eng. Des*., 2009, 239(4): 628-640.

[7] Ramberg W and Osgood W R. Description of stress-strain curves by three parameters[J]. *Technical Report Archive & Image Library*, 1943(902).

[8] Ueda Y, Shi Y, Sun S and H Murakawa. Effect of crack depth and strength mis-matching on the relation between J-integral and CTOD for welded tensile specimens[J]. *Trans. JWRI*, 1997, 26(1): 133-140.

[9] ABAQUS. ABAQUS/Standard User's Manual Version 6.14[Z]. ABAQYS Inc, 2015.

[10] Peng Q, Xue H, Hou J, Sakaguchi K, Takeda Y, Kuniya J and Shoji T. Role of water chemistry and microstructure in stress corrosion cracking in the fusion boundary region of an Alloy 182-A533B low alloy steel dissimilar weld joint in high temperature water[J]. *Corros. Sci*., 2011, 53(12): 4309-4317.

[11] Zhao L, Xue H, Jiao K and Tang W. Analysis of Interface Fracture on Piping Welded Joint with Continuous Material Properties[C]. *Fourth International Conference on Digital Manufacturing and Automation. IEEE*, 2013: 207-210.

[12] Peng, Q, Kwon, J, Shoji T. Development of a fundamental crack tip strain rate equation and its application to quantitative prediction of stress corrosion cracking of stainless steels in high temperature oxygenated water[J]. *J. Nucl. Mater.*, 2004, 324(1): 52-61.

[13] Kim Y J, Kim J S, Cho S M and Kim Y J. 3-D constraint effects on J, testing and crack tip constraint in M(T), SE(B), SE(T) and C(T) specimens: numerical study[J]. *Eng. Fract. Mech*., 2004, 71(9): 1203-1218.